# Supramolecular Nanostructures from Self-Assembly of T-Shaped Rod Building Block Oligomers

Zhuoshi Wang,[1] Junjie Cui,[1] Yongri Liang,[2] Tie Chen,[1] Myongsoo Lee,[3] Bingzhu Yin,[1] Long Yi Jin[1]

[1]Key Laboratory for Organism Resources of the Changbai Mountain and Functional Molecules, Ministry of Education, Department of Chemistry, College of Science, Yanbian University, No. 977, Gongyuan Road, Yanji 133002, People's Republic of China
[2]Beijing National Laboratory for Molecular Sciences, Joint Laboratory of Polymer Science and Materials, Institute of Chemistry, Chinese Academy of Sciences, Beijing 100190, People's Republic of China
[3]State Key Laboratory of Supramolecular Structure and Materials, Jinlin University, Changchun 130012, People's Republic of China
Correspondence to: M. Lee (E-mail: mslee@jlu.edu.cn) L. Y. Jin (E-mail: lyjin@ybu.edu.cn)

**ABSTRACT**: T-shaped coil–rod–coil oligomers, consisting of a dibenzo[a,c]phenazine unit and phenyl groups linked together with acetylenyl bonds at the 2,7-position of dibenzo[a,c]phenazine as a rigid segment have been synthesized. The coil segments of these new molecules composed of poly(ethylene oxide) (PEO)–poly(propylene oxide) (PPO) incorporating lateral methyl groups between the rod and coil segment and two flexible alkyl groups connecting with the rigid segment at the 4,6-position of dibenzo[a,c]phenazine, respectively. The experimental results reveal that the length of the flexible PEO coil chain influence construction of various supra-nanostructures from lamellar structure to rectangular columnar structure. It is also shown that introduction of different length of alkyl side chain groups in the backbone of the T-shaped molecules affect the self-organization behavior to form hexagonal perforate layer or oblique columnar structures. In addition, lateral methyl groups attached to the surface of rod and coil segments, dramatically influence the self-assembling behavior in the crystalline phase. T-shaped molecules containing a lateral methyl group at the surface of rod and PEO coil segments, self-assemble into 3D body-centered tetragonal structures in the crystalline phase, while molecules without a lateral methyl group based on PEO coil chain self-organize into 2D oblique columnar crystalline structures. © 2013 Wiley Periodicals, Inc. J. Polym. Sci., Part A: Polym. Chem. **2013**, *51*, 5021–5028

**KEYWORDS**: rod–coil; SAXS; self-assembly; supramolecular structure; T-shaped

**INTRODUCTION** Accurate control of the supramolecular nanostructures with a well-defined shape, through self-assembly of functional molecules or polymers is an efficient way to produce supramolecular ordered nanomaterials.[1–4] An example of a self-assembling architectures is provided by coil–rod–coil block copolymers, which have a strong capacity to form various supramolecular nanostructures, such as lamellar, hexagonal or tetragonal perforated layer, columnar, 3D bundles structures, and so on.[5–8] These periodic nanostructures of rod–coil molecules are created by microphase separation of the rod and coil blocks, due to occurrence of the mutual repulsion of the dissimilar blocks and the packing constraints imposed by the connection of each block.[9–12] To balance these competing parameters, rod–coil molecules self-organize into a diverse supramolecular structures, which can be controlled by tuning of the rod to coil volume fraction,[13,14] the number of grafting sites per rod,[15] rod anisotropy, coil cross-sectional area and incorporating the side groups into a rod block.[16,17] The self-assembling behavior of rod–coil copolymers based on various shapes of rod building block including Y-shaped, T-shaped, O-shaped, K-shaped, propeller-shaped, and dumbbell-like have been reported by Percec, Lee, and other research groups.[18–24] The ordered nanostructures of rod–coil molecules have been created by introduction of diverse flexible coil segments into the various shaped rod building block and produce unique self-assembling or aggregation structures.[25–27] Cho and Lee reported that coil-cross sectional area of rod–coil molecules is one of the main parameter of self-assembling nanostructures. The self-organized structure of rod–coil molecules conversed from a hexagonal perforated layer structure to 3D discrete rod bundles as a function of coil-cross sectional area

Additional Supporting Information may be found in the online version of this article.

at the constant coil to rod volume ratio.[28] In addition, Huang et al. demonstrated that the cross-sectional area of flexible chain can adjust the rotation angle of shearing motion between rods with different dendritic PEO chains to self-assemble into supramolecular rectangular columnar and oblique columnar structures.[29] Recently, we have illustrated copolymers with short alkyl side groups incorporating in the middle of rod building block, dramatically influence construction of ordered nanostructures from lamellar or hexagonal perforated layer structures to a rectangular columnar structure, depending on the molecular structure and shapes.

Dibenz[a,c]phenazine (DBP) is a structural analogue of the dibenz[a,c]-anthracene. Diiodo-DBP substituted at 2,7 position, which is promising to give skeletal rigidity, electron affinity, and thermal stability,[30] is able to be synthesized and suitable consists of T-shaped rod building block copolymers for organic electrophoto materials. Hence, there is specifically a growing interest in study parameters on phase behavior and the correlation between the supramolecular nanostructures of T-shaped rod building block copolymers and the lateral methyl groups attached to the surface of rod and coil segments.

In this article, we report synthesis and self-assembling behavior of T-shaped new oligomers (see Scheme 1). The self-assembly of these new materials, in particular, the structural effects of the molecular shape, the length of the poly(-ethylene oxide) (PEO) coil and the lateral methyl groups at the surface of the rod and coil domains are investigated by differential scanning calorimetry (DSC) and small-angle X-ray scattering (SAXS) in the solid state.

## EXPERIMENTAL

### Materials

9,10-Phenanthrenequinone (95%), *N*-iodosuccinimide (97%), and trifluoroacetic acid (99%) were purchased from Alfa Aesar. Benzoyl peroxide (97%), ethylene glycol (99.8%), nitrobenzene (99%), *tert*-butyllithium (1.7 M in pentane), 1-iodohexane (98%), 1-iododdodecane (98%), 1-iodooctadecane (95%), (1R)-(−)−10-camphorsulfonic acid (98%), and toluene-*p*-sulfonyl chloride (TsCl, 99%) (all from Aldrich) were used as received.

### Techniques

^{1}H NMR spectra was recorded from CDCl$_3$ solution on a Bruker AM 300 spectrometer. Column chromatography (silica gel 100–200) was used to check the purity of the products. A Perkin Elmer Pyris Diamond differential scanning calorimeter was used to determine the thermal transitions with the maxima and minima of their endothermic or exothermic peaks, controlling the heating and cooling rates to 10 °C/min. X-ray scattering measurements were performed in transmission mode with synchrotron radiation at the 1W2A X-ray beam line at Beijing Accelerator Laboratory. MALDI-TOF-MS was performed on a Perceptive Biosystems Voyager-DE STR using a 2-cyano-3-(4-hydroxyphenyl) acrylic acid (CHCA) as matrix.

### Synthesis of Precursors 4–8

These compounds were prepared using a series of reactions. For detailed synthetic procedures, see Supporting Information.

### Synthesis of the T-Shaped Coil–Rod–Coil Oligomers (1–3)

These oligomers were synthesized by the same synthetic procedures. A representative example was described for **2b**. Compound **8a** (0.29 g, 0.5 mmol), Compound **9b** (0.80 g, 1.36 mmol), CuI (38 mg, 0.2 mmol), and Pd(PPh$_3$)$_4$ (115.5 mg, 0.1 mmol) were dissolved in absolute THF (30 mL) and Et$_3$N (20 mL). The mixture was refluxed for 48 h under N$_2$ and keeps it away from the light. Then, it was concentrated by evaporation and washed with water. The mixture was extracted with dichloromethane and dried over anhydrous magnesium sulfate and filtered. After the solvent was removed in a rotary evaporator, the crude product was purified by silica gel chromatography (EA: CH$_3$OH, 30:1 to 10:1) to yield 0.18 g of yellow solid (25.7%). The product was further purified by recycle gel permeation chromatography and dried for elemental analysis.

^{1}H NMR (300 MHz, CDCl$_3$, δ, ppm): 9.44 (s, 2H), 8.33 (dd, $J = 6.5$ Hz, 3.4 Hz, 4H), 7.85 (dd, $J = 6.5$ Hz, 3.4 Hz, 4H), 7.56 (d, $J = 8.8$ Hz, 4H), 6.96 (d, $J = 8.8$ Hz, 4H), 4.19 (t, $J = 9.0$ Hz 4H), 3.90 (t, $J = 9.0$ Hz, 4H), 3.63–3.68 (m, 56H), 3.38 (s, 6H), 2.94 (t, $J = 7.6$ Hz, 4H), 1.77 (p, $J = 7.6$ Hz, 4H), 1.25–1.50 (m, 12H), 0.86 (t, $J = 6.7$ Hz, 6H). Anal. Calcd for C$_{82}$H$_{112}$N$_2$O$_{18}$: C, 69.66; H, 7.98; N, 1.98. Found: C, 69.72; H, 7.93; N, 1.90. MALDI-TOF-MS m/z [M + Na]$^+$ 1437.
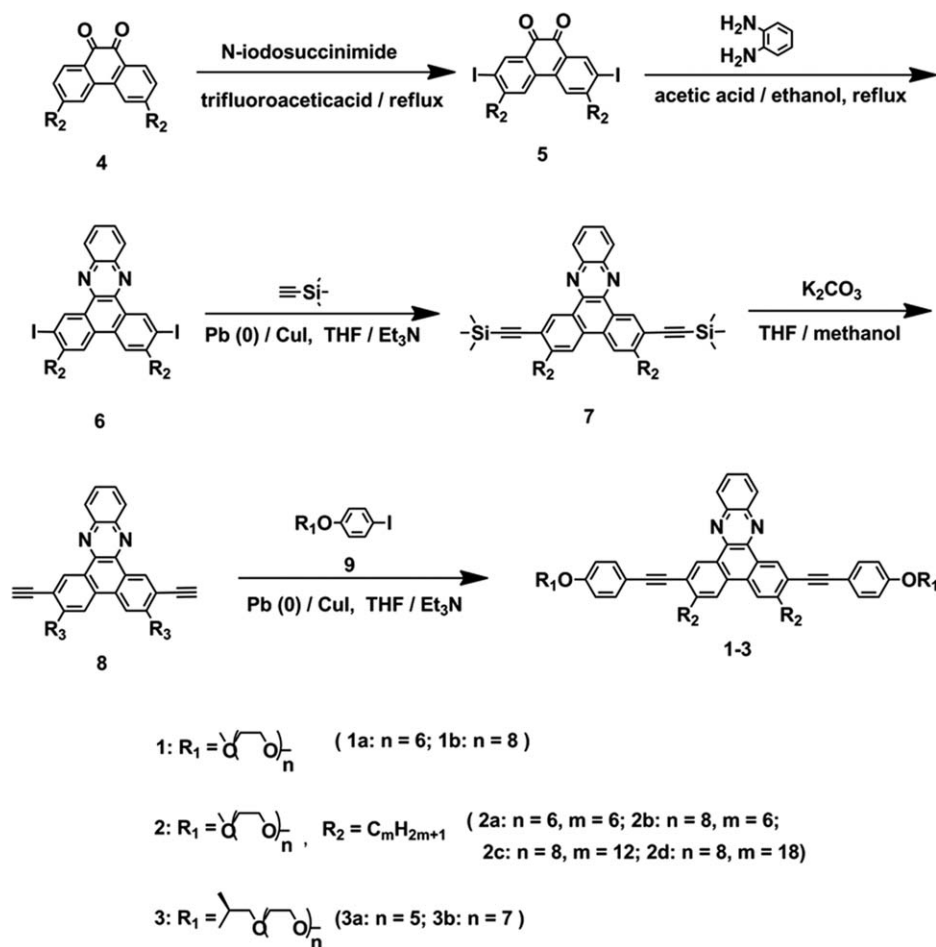
#### *Oligomer 1a*

Yield: 36.2%; ^{1}H NMR (300 MHz, CDCl$_3$, δ, ppm): 9.44 (s, 2H), 8.33 (dd, $J = 6.5$ Hz, 3.4 Hz, 4H), 7.85 (dd, $J = 6.5$ Hz, 3.4 Hz, 4H), 7.56 (d, $J = 8.8$ Hz, 4H), 6.96 (d, $J = 8.8$ Hz, 4H), 4.20 (t, $J = 9$ Hz 4H), 3.91 (t, $J = 9$ Hz, 4H), 3.66–3.75 (m, 42H), 3.38 (s, 6H). Anal. Calcd for C$_{62}$H$_{72}$N$_2$O$_{14}$: C, 69.64; H, 6.79; N, 2.62. Found: C, 69.59; H, 6.81; N, 2.55. MALDI-TOF-MS m/z [M]$^+$ 1070, [M + Na]$^+$ 1093, [M + K]$^+$ 1108.

#### *Oligomer 1b*

Yield: 28.6%; ^{1}H NMR (300 MHz, CDCl$_3$, δ, ppm): 9.42 (d, $J = 8.4$ Hz, 2H), 8.73 (s, 2H), 8.41 (dd, $J = 6.5$ Hz, 3.4 Hz, 2H), 7.89 (dd, $J = 6.7$, 3.4 Hz, 4H), 7.58 (d, $J = 8.8$ Hz, 4H), 6.96 (d, $J = 8.8$ Hz, 4H), 4.19 (t, $J = 9.0$ Hz 4H), 3.90 (t, $J = 9.0$ Hz, 4H), 3.66–3.75 (m, 56 H), 3.37 (s, 6H). Anal. Calcd for C$_{70}$H$_{88}$N$_2$O$_{18}$: C, 67.51; H, 7.12; N, 2.25. Found: C, 67.42; H, 7.16; N, 2.18. MALDI-TOF-MS m/z [M]$^+$ 1245, [M + Na]$^+$ 1267.

#### *Oligomer 2a*

Yield: 31.2%; ^{1}H NMR (300 MHz, CDCl$_3$, δ, ppm): 9.44 (s, 2H), 8.33 (dd, $J = 6.5$ Hz, 3.4 Hz, 4H), 7.85 (dd, $J = 6.5$ Hz, 3.4 Hz, 4H), 7.56 (d, $J = 8.8$ Hz, 4H), 6.96 (d, $J = 8.8$ Hz, 4H), 4.19 (t, $J = 9.0$ Hz 4H), 3.90 (t, $J = 9.0$ Hz, 4H), 3.63–3.68 (m, 40H), 3.38 (s, 6H), 2.94 (t, $J = 7.6$ Hz, 4H), 1.77 (p, $J = 7.6$ Hz, 4H), 1.25–1.50 (m, 12H), 0.86 (t, $J = 6.7$ Hz, 6H). Anal. Calcd for C$_{74}$H$_{96}$N$_2$O$_{14}$: C, 71.82; H, 7.82; N, 2.26. Found: C,

**SCHEME 1** Synthetic route of oligomers **1–3**.

71.86; H, 7.78; N, 2.19. MALDI-TOF-MS m/z $[M]^+$ 1237, $[M + Na]^+$ 1260.

### Oligomer 2c
Yield: 27.8%; $^1H$ NMR (300 MHz, CDCl$_3$, $\delta$, ppm): 9.47 (d, $J = 8.3$ Hz, 2H), 8.33 (dd, $J = 6.5$ Hz, 3.4 Hz, 4H), 7.79–7.84 (m, 2H), 7.57 (d, $J = 8.8$ Hz, 4H), 6.96 (d, $J = 8.8$ Hz, 4H), 4.19 (t, $J = 9.0$ Hz 4H), 3.90 (t, $J = 9.0$ Hz, 4H), 3.66–3.75 (m, 56H), 3.37 (s, 6H), 2.94 (t, $J = 7.6$ Hz, 4H), 1.77 (p, $J = 7.6$ Hz, 4H), 1.25–1.50 (m, 36H), 0.86 (t, $J = 6.7$ Hz, 6H). Anal. Calcd for C$_{94}$H$_{136}$N$_2$O$_{18}$: C, 71.36; H, 8.66; N, 1.77, Found: C, 71.42; H, 8.72; N, 1.68. MALDI-TOF-MS m/z $[M]^+$ 1582, $[M + Na]^+$ 1605, $[M + K]^+$ 1621.

### Oligomer 2d
Yield: 33.7%; $^1H$ NMR (300 MHz, CDCl$_3$, $\delta$, ppm): 9.42 (d, $J = 8.4$ Hz, 2H), 8.73 (s, 2H), 8.41 (dd, $J = 6.5$ Hz, 3.4 Hz, 2H), 7.81 (dd, $J = 6.7$, 3.4 Hz, 4H), 7.56 (d, $J = 8.8$ Hz, 4H), 6.96 (d, $J = 8.8$ Hz, 4H), 4.19 (t, $J = 9.0$ Hz 4H), 3.90 (t, $J = 9.0$ Hz, 4H), 3.66–3.75 (m, 56 H), 3.37 (s, 6H), 2.94 (t, $J = 7.6$ Hz, 4H), 1.77 (p, $J = 7.6$ Hz, 4H), 1.25–1.50 (m, 60H), 0.86 (t, $J = 6.7$ Hz, 6H). Anal. Calcd for C$_{106}$H$_{160}$N$_2$O$_{18}$: C, 72.73; H, 9.21; N, 1.60. Found: C, 72.68; H, 9.28; N, 1.69. MALDI-TOF-MS m/z $[M + Na]^+$ 1773.

### Oligomer 3a
Yield: 34.2%; $^1H$ NMR (300 MHz, CDCl$_3$, $\delta$, ppm): 9.53 (d, $J = 1.7$ Hz, 2H), 8.50 (d, $J = 8.6$ Hz, 2H), 8.39–8.35 (m, 2H), 7.90 (dd, $J = 8.3$, 1.7 Hz, 4H), 7.57 (d, $J = 8.8$ Hz, 4H), 6.96 (d, $J = 8.8$ Hz, 4H), 4.56–4.64 (m, 2H), 3.66–3.75 (m, 44H), 3.37 (s, 6H), 1.35 (d, $J = 6.2$ Hz, 6H). Anal. Calcd for C$_{64}$H$_{76}$N$_2$O$_{14}$: C, 70.05; H, 6.98; N, 2.55, Found: C, 70.13; H, 6.90; N, 2.46. MALDI-TOF-MS m/z $[M]^+$ 1097.

### Oligomer 3b
Yield: 36.7%; $^1H$ NMR (300 MHz, CDCl$_3$, $\delta$, ppm): 9.39 (s, 2H), 8.39 (d, $J = 8.6$ Hz, 2H), 8.30 (dd, $J = 6.5$ Hz, 3.4 Hz, 2H), 7.83–7.86 (m, 4H), 7.56 (d, $J = 8.7$ Hz, 4H), 6.97 (d, $J = 8.7$ Hz, 4H), 4.76–4.64 (m, 2H), 3.66–3.75 (m, 60H), 3.37 (s, 6H), 1.34 (d, $J = 6.2$ Hz, 6H). Anal. Calcd. for C$_{72}$H$_{92}$N$_2$O$_{18}$: C, 67.90; H, 7.28; N, 2.20. Found: C, 67.95; H, 7.34; N, 2.26. MALDI-TOF-MS m/z $[M + Na]^+$ 1296.

### RESULTS AND DISCUSSION

#### Synthesis of T-Shaped Oligomers 1–3
The synthetic route of T-shaped coil–rod–coil oligomers, consisting of a dibenzo[a,c]phenazine unit and phenyl groups linked together with acetylenyl bonds at the 2,7-position of
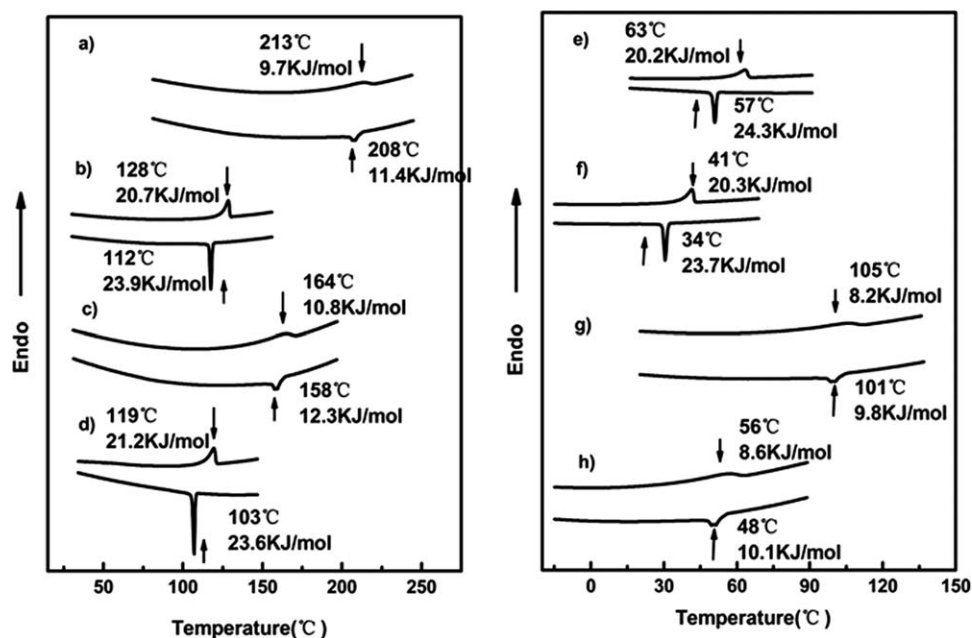
**FIGURE 1** DSC traces (10 °C/min) recorded during the second heating scan and the first cooling scan of the series of Compounds **1**, **2**, and **3**; (a) **1a**, (b) **2a**, (c) **1b**, (d) **2b**, (e) **2c**, (f) **2d**, (g) **3a**, and (h) **3b**.

dibenzo[a,c]phenazine as a rigid segment was outlined in Scheme 1. Compound **8** was obtained from successive reactions of radical bromination reactions, iodine reaction, coupling reaction, sonogashira coupling reaction, demethylation, using 3,6-dialkylphenanthrenequinone as starting materials. Molecule **9** was synthesized according to the literature reported elsewhere.[31,32] Coil–rod–coil Molecules **1–3** successfully synthesized through Sonogashira coupling reaction of Compounds **8** and **9**. The resulting molecules were purified by silica gel column chromatography and then further purified by recycling preparative high-performance liquid chromatography (HPLC). The structure of molecules **1–3** were characterized by ^{1}H NMR and matrix-assisted laser desorption ionization time-of-flight (MALDI-TOF) mass spectroscopy and were shown to be in full agreement with the structure presented in Scheme 1.

### Structures of Bulk State
Self-assembled structures of the oligomers were investigated by means of DSC and SAXS in the solid state. Figure 1 shows the DSC heating, cooling traces and thermal transitions of the oligomers **1a–1b**, **2a–2d**, and **3a–3b**. The transition temperatures together with the corresponding enthalpy changes (in brackets) determined from the DSC scans are summarized in Table 1. As shown in Table 1, the melting transition temperatures of the coil–rod–coil molecules decrease as the PEO coil length increase. Molecules **1a** and **1b** with 6 and 8 ethylene oxide repeating units, connected with a dibenzo[a,c]phenazine unit and phenyl groups linked together with acetylenyl bonds at the 2,7-position of dibenzo[a,c]phenazine, show an ordered bulk-state organization, which transform into an isotropic liquid at 213 °C and 164 °C. Melting points together with enthalpy changes of Molecules

**3a** and **3b**, composed of PEO coil segment, incorporating lateral methyl groups between the rod and coil segment, significantly decrease than Molecules **1a** and **1b**, indicative of change of driving force by incorporating methyl groups in the surface of rod and coil domains. Molecules **2a–2d**, containing two flexible alkyl groups connecting with the rigid segment at the 4,6-position of dibenzo[a,c]phenazine melt into an optically isotropic mesophase at 128 °C, 119 °C, 63 °C, and 41 °C, respectively, and also show strong effect of side groups for driving force of molecular assembly. The results clearly interpret that adjusting flexible chain length, side groups at the surface of rod and coil domains and in the center of rod segment lead to reduce phase transition temperatures.

**TABLE 1** Thermal Transitions of Molecules **1a–1b**, **2a–2d**, and **3a–3b** (Data from the Second Heating and the First Cooling Scans)

| Molecular | Phase Transition (°C) and Corresponding Enthalpy Changes (kJ mol$^{-1}$) | |
|---|---|---|
| | Heating | Cooling |
| 1a | k 213 (9.7) i | i 208 (11.4) k |
| 1b | k 164 (10.8) i | i 158 (12.3) k |
| 2a | k 128 (20.7) i | i 112 (23.9) k |
| 2b | k 119 (21.2) i | i 103 (23.6) k |
| 2c | k 63 (20.2) i | i 57 (24.3) k |
| 2d | k 41 (20.3) i | i 34 (23.7) k |
| 3a | k 105 (8.2) i | i 101 (9.8) k |
| 3b | k 56 (8.6) i | i 48 (10.1) k |
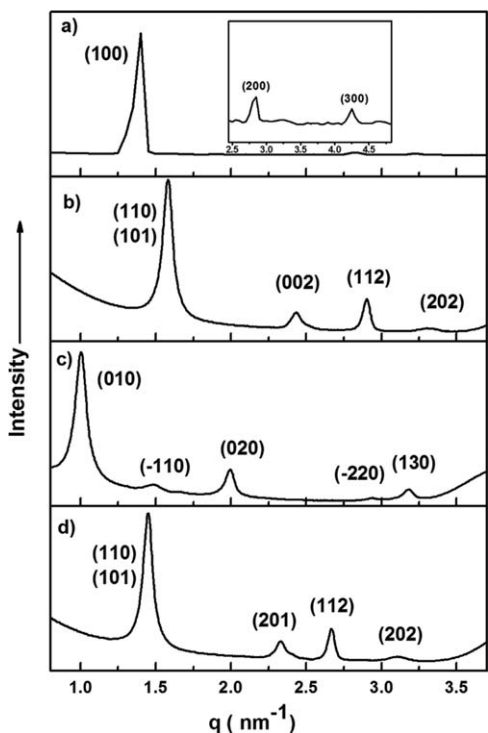
**FIGURE 2** Small-angle X-ray diffraction patterns of the rod–coil oligomers measured in their solid state; (a) **1a**, (b) **3a**, (c) **1b**, and (d) **3b**.

To identify the detailed self-organizing structures, X-ray scattering studies were performed. In the crystalline phases of **1a**, the small angle X-ray diffraction patterns display several sharp reflections which correspond to equidistant q-spacings and thus index to a lamellar lattice [Fig. 2(a)]. The layer spacing at the lower temperature crystalline phase of 60 Å is very close to the corresponding estimated molecular length (60.4 Å), indicative of a monolayer lamellar structure, in which rod segments are fully interdigitated.

In contrast to **1a**, coil–rod–coil Molecule **1b** based on the longer coil length displayed a distinct nanostructure. The X-ray diffraction patterns of **1b** shown in Figure 2(c) can be indexed as the (010), (−110), (020), (−220), and (130) that correspond to a two-dimensional rectangular columnar structure with lattice constants $a = 63$ Å and $b = 58$ Å. From the experimental values of the unit cell parameters ($a$, $b$, $c$) and the density ($\rho = 1.02$), the average number ($n$) of molecules per cross-sectional slice of the column is calculated about 8, according to following equation, where $M_w$ is the molecular weight and $N_A$ is Avogadro's number.

$$n = (abc \times \sin \gamma) \times \rho \times N_A / M_w \qquad (1)$$

The results described above demonstrate the capability of manipulating the supramolecular structure by the different lengths of flexible PEO chains more affect self-assembling behavior for T-shaped rigid building block [Fig. 2(a,c)]. The tendency of a 1D-lamellar phase to transform into a 2D-columnar phase is consistent with the results from n-shaped

rod–coil systems reported by our laboratory.[25] The variation in the supramolecular structure can be rationalized by considering the microphase separation between the dissimilar parts of the molecule and the space-filling requirement of the flexible PEO chains.

To investigate the effect of the alkyl lateral chains in the middle of rod building block to the self-assembly of the rigid-flexible molecules, we designed and synthesized the series of molecules **2a–2d**, incorporating alkyl lateral chains in the center of rod segment, and hexaethylene glycol monomethyl ether and octaethylene glycol monomethyl ether as coil segment, respectively.

In comparison with Molecule **1a**, **2a** structure has extra two hexyl groups at the 3,6-position of dibenzo[a,c]phenazine. In the crystalline phase for Molecule **2a**, SAXS patterns display two main peaks together with five reflections, as shown in Figure 3(a). The observed reflections can be indexed as the (101), (002), (100), (110), (202), (113), and (210) planes for 3D hexagonal symmetry (P63/mmc space group symmetry) with lattice constants $a = 54.4$ Å and $c = 78$ Å (see Supporting Information Table S1). An interesting point to be noted is that the peak intensity associated with the (002) reflection appears to be the most intense, implying that the fundamental structure is lamellar. The average number ($n$) of molecules per micelle can be calculated to be 71, according to eq 1.
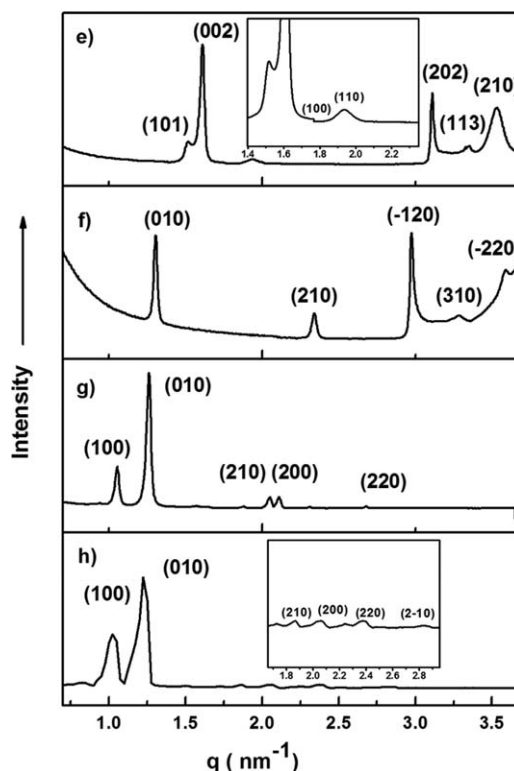


**FIGURE 3** Small-angle X-ray diffraction patterns of the rod–coil oligomers measured in their solid state; (a) **2a**, (b) **2b**, (c) **2c**, and (d) **2d**.

In contrast to **1b**, Molecules **2b**, **2c**, and **2d** incorporate extra two hexyl, dodecyl, and octadecyl groups, at the 3,6-position of dibenzo[a,c]phenazine respectively. The SAXS pattern of Molecule **2b** shows a number of reflections that can be indexed as the (010), (210), (−120), (310), and (−220) reflections of a 2D oblique columnar structure with the lattice parameters $a = 54.0$ Å, $c = 48.3$ Å, characteristic angle $\gamma = 81°$ [Fig. 3(b)]. The average number ($n$) of molecules per cross-sectional slice of the column can be calculated to be 6, according to eq 1. Similar to molecules **2b**, **2c**, and **2d** with longer alkyl lateral chain in the middle of T-shaped rod building block give rise to slight structural changes for the self-assembling behavior. Figure 3(c,d) shows X-ray diffraction patterns for Molecules **2c** and **2d** recorded at room temperature, the several patterns of **2c** can be indexed as the (100), (010), (210), (200), and (220) planes for a two-dimensional oblique columnar structure with lattice parameters $a = 6.34$ nm, $b = 5.3$ nm, $\gamma = 70°$ (see Supporting Information Table S2). SAXS patterns of **2d** also can be characterized as the (100), (010), (210), (200), (220), and (2−10) planes for a two-dimensional oblique columnar structure with lattice constants $a = 68.4$ Å, $b = 57.8$ Å, $\gamma = 63°$. The results described above, show that the value of lattice parameters (a and b) of oblique columnar structures increases and the characteristic angle decreases systematically as increasing the lengths of alkyl lateral chain in the rod building block. The variation of lattice parameters can be rationalized by considering both the steric repulsion between the alkyl lateral chains and the nanophase separation between the dissimilar parts of the molecules. The elongated lateral chains in the middle of rod segment lead to loose packing of the extended rod segments, which are able to decrease the molecular interaction of $\pi$–$\pi$ stacking and can therefore induce the formation of diverse supramolecular nanostructures, compared to nonlateral-chain molecules.

Molecules **3a** and **3b** were synthesized to investigate the effect of chiral methyl group incorporated at the surface of rod and coil segments for self-assembly of T-shaped coil–rod–coil molecules. The SAXS pattern of Molecule **3a** shows a sharp, high intensity reflection at a low angle together with a number of sharp reflections of low intensity at higher angles [Fig. 2(b)]. These reflections can be indexed as the (100), (010), (210), (−120), (310), and (−220) planes for a three-dimensional body-centered tetragonal structure with lattice constants of $a = 56.1$ Å and $c = 51.6$ Å ($c/a = 0.92$). To describe the detailed supramolecular structure, it is desirable to calculate the number of molecules per micelle. From the lattice constants and the densities, the average number ($n$) of molecules per micelle can be calculated about 46, according to eq 2, where $M_w$ is the molecular weight, $\rho$ is molecular density, and $N_A$ is Avogadro's number.

$$n = a^2 c \frac{N_A \rho}{2 M_w} \qquad (2)$$

For the body centered tetragonal assembly structure of T-shaped rod building block Molecule **3a**, the inner core of micelle is constituted by the discrete rod bundle that is encapsulated with phase separated PEO coils, which give rise to form the nonspherical oblate aggregate. Similar to Molecule **3a**, SAXS experiments of Molecule **3b** [Fig. 2(d)] also can be indexed as a three-dimensional, body-centered, tetragonal lattice with lattice constants of $a = 61.3$ Å and $c = 56.4$ Å ($c/a = 0.92$). The average number ($n$) of molecules in each supramolecular aggregate is ∼52, according to eq 2.

From the SAXS analysis of **3a** and **3b**, it is pointed out that methyl groups incorporated at the surface between the rod and coil segment, dramatically influence self-organization of T-shaped rod–coil molecules. Compare with molecules **3a** and **3b**, molecules **1a** and **1b**, containing the same coil segment (PEO) and similar volume fraction of coil segment are formed lamellar and hexagonal perforate layer structures in the crystalline phase, respectively. While, Molecules **3a** and **3b** connected with two methyl group at the surface of rod and coil domains display body centered tetragonal structure in the crystalline phase. This variation of phase behavior is caused by methyl groups in the surface of the rod and coil segments, leading to loose packing of the extended rod segments, which are also able to decrease driving force of $\pi$–$\pi$ stacking and can therefore produce various supramolecular nanostructures compared to nonlateral-chain molecules **1a** and **1b**.

It is noteworthy that we have reported synthesis and self-assembly of coil–rod–coil molecules, consisting of four or five biphenyls linked together with ether bonds as a rod segment and poly(propylene oxide) (PPO) with a degree of polymerization (DP) of 12 or PEO with a DP of 17 as coil segments. Various supramolecular nanostructures are constructed by these molecules, although, they have the same rod segment and equal volume fraction of the coil segment but have different coil segment. The variation in the self-assembly behavior of these molecules can be rationalized by considering the difference in coil cross-sectional area between PPO and PEO coil segments. In contrast to these molecules, Molecules **3a** and **3b**, which have only two methyl groups linked with PEO coil chain in the surface of rod and coil segment, significantly affect self-assembling behavior of rod coil molecular system, hence, the density of the coil/rod interface is probably one of major parameters for construction of various supramolecular nanostructures for application in materials science. These results imply that controlling steric hindrance at the rod/coil interface could govern supramolecular rod assembly in coil–rod–coil systems.

In summary, it is interesting that incorporating methyl or other alkyl groups in the surface of coil and rod domains or short lateral alkyl chains in the center of rod domain can construct various supramolecular nanostructures for T-shaped rod–coil molecular systems. Based upon the data presented so far, a schematic representation of the self-assembled structures of **1a–1b**, **2a–2d**, and **3a–3b** is illustrated in Figure 4.
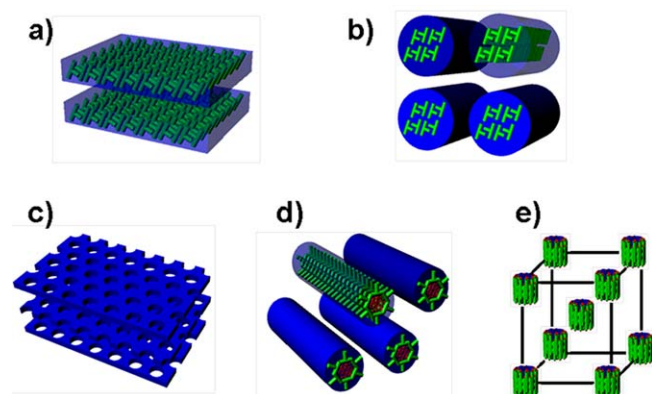
**FIGURE 4** Schematic representation of self-assembly of (a) monolayer structure for **1a**, (b) rectangular columnar structure for **1b**, (c) perforated lamellar structure for **2a**, (d) oblique columnar structures for **2b**, **2c**, **2d**, and (e) the body-centered tetragonal superlattice for **3a**, **3b**. [Color figure can be viewed in the online issue, which is available at wileyonlinelibrary.com.]

## Aggregation Behavior of Molecule 3 in Aqueous Solution

Molecules **1–3** can be considered as a novel class of amphiphiles due to these molecules consist of hydrophilic PEO flexible chains and hydrophobic T-shaped rigid aromatic segments. To study the effect of the enantiomerically pure side chain for self-assembly of T-shaped rod–coil molecules, aggregation behavior of molecules **1–3** was subsequently studied in aqueous solution using circular dichroism (CD) spectra. As shown in Figure 5, CD spectra of Molecules **3a** and **3b** with chiral groups at the coil segments showed a strong positive and negative cotton effect in their aqueous solutions, while no CD signals could be detected for molecules **1** and **2** with a lack of chiral groups, indicating the helical stacks of the rod segments caused by chiral transfer from coil segments. To obtain detailed information of self-assembling behavior of Molecule **3**, UV/vis and fluorescence experiments were performed in aqueous solution (see Fig. 6). The absorption spectra of **3a** and **3b** in aqueous solution
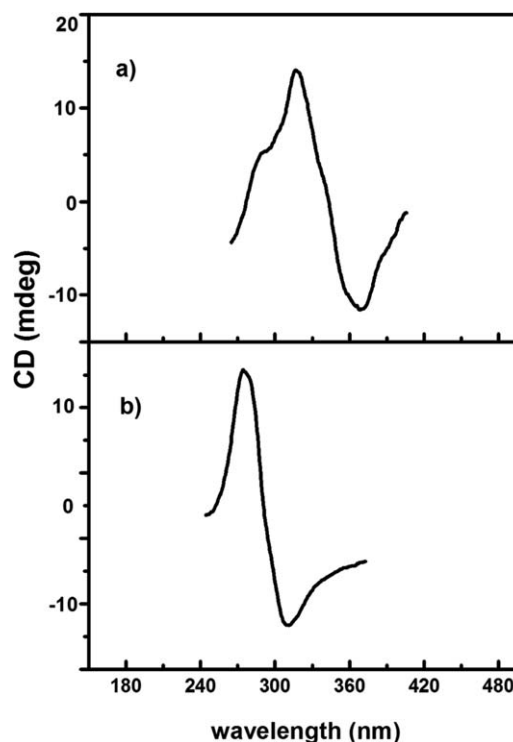


**FIGURE 5** (a) CD spectrum of **3a** in aqueous solution ($2 \times 10^{-5}$ M) and (b) CD spectrum of **3b** in aqueous solution ($2 \times 10^{-5}$ M).

(0.02 wt %) exhibit a blue-shifted absorption maxima compared to those of chloroform solutions. This is maybe caused by the corporative effect between the hydrophilic and hydrophobic interactions and the $\pi-\pi$ stacking interactions between the aromatic segments. The fluorescence spectra of **3a** and **3b** in chloroform solution (0.02 wt %) exhibit a strong emission maximum at 429 and 454 nm, respectively. However, the emission maximum in aqueous solution is significantly quenched, strongly indicative of aggregation of the conjugated rod segments. Further studies of self-assembling behavior in aqueous solution of molecules **1–3** and the series of rod–coil molecules with chiral methyl groups at the
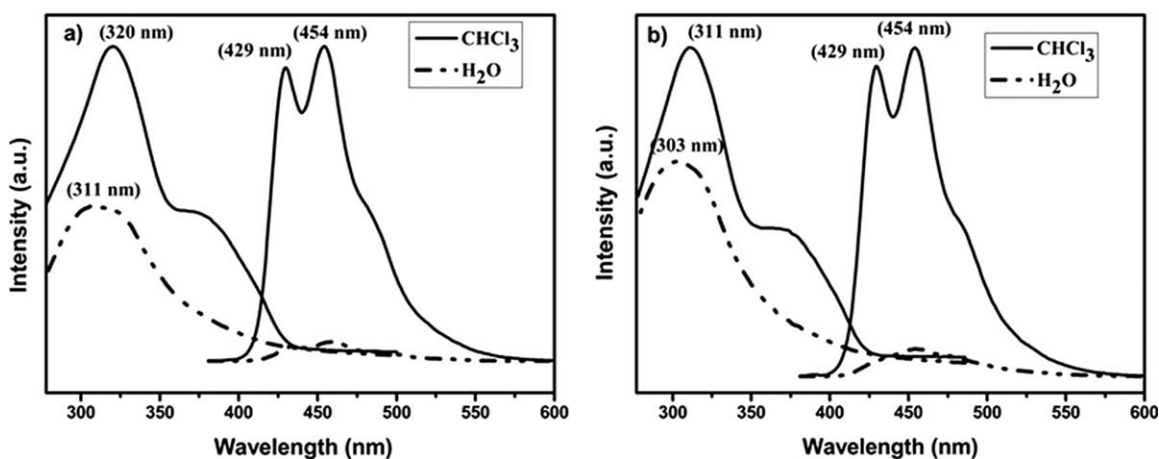


**FIGURE 6** (a) Absorption and emission spectra of **3a** in chloroform and aqueous solution (0.002 wt %), (b) Absorption and emission spectra of **3b** in chloroform and aqueous solution (0.002 wt %).

coil segments and of the electro-optic properties of these new materials, are underway.

## CONCLUSIONS

T-shaped coil–rod–coil oligomers, consisting of a dibenzo[a,c]-phenazine unit and phenyl groups linked together with acetylenyl bonds at the 2,7-position of dibenzo[a,c]phenazine as a rigid segment were synthesized. The coil segments of these new molecules composed of PEO–PPO incorporating lateral methyl groups between the rod and coil segment and two flexible alkyl groups connecting with the rigid segment at the 4,6-position of dibenzo[a,c]phenazine respectively. The self-assembling behavior of these molecules was investigated in the crystalline phase by means of DSC and SAXS. Molecule **1a** with a short length of coils self-assembles into lamellar crystalline, while the Molecule **1b** with longer length of coils aggregates to a 2D rectangular columnar structure. Molecules **2a–2d** and **3a–3b**, incorporating methyl or alkyl groups in the surface of coil and rod segments or in the center of rod building block, assemble into supramolecular aggregates that spontaneously organize into a perforated lamellar structure, oblique columnar structures and 3D body-centered tetragonal structures respectively. Remarkably, in combination with the lateral methyl group in the surface of rod and coil domains of molecules **1a** or **1b**, the supramolecular structures are dramatically conversed from lamellar structure or rectangular columnar structure into 3D body-centered tetragonal structure. The experimental results reveal that the length of the flexible PEO coil chain influence construction of various supra-nanostructures. Furthermore, introduction of different length of alkyl side chain groups in the center of rod segment or incorporating lateral methyl groups attached to the surface of rod and coil segments significantly affect the self-assembly behavior in the crystalline phase for T-shape molecules. The strategy described here regarding the incorporation of methyl groups in the surface of rod and coil segments could induce the formation of various supramolecular nanostructures in rod–coil molecular architecture.

## REFERENCES AND NOTES

**1** G. B. Ligthart, R. P. Sijbesma, E. W. Meijer, *J. Am. Chem. Soc.* **2005**, *127*, 810–811.

**2** W. Jin, T. Fukushima, A. Kosaka, M. Niki, N. Ishii, T. Aida, *J. Am. Chem. Soc.* **2005**, *127*, 8284–8285.

**3** F. Hoeben, P. Jonkheijm, E. W. Meijer, A. P. Schenning, *Chem. Rev.* **2005**, *105*, 1491–1546.

**4** D. A. Wilson, C. J. Wilson, C. Moldoveanu, A. Resmerita, P. Corcoran, L. M. Hoang, B. M. Rosen, V. Percec, *J. Am. Chem. Soc.* **2010**, *132*, 1800–1801.

**5** B. M. Rosen, C. J. Wilson, D. A. Wilson, M. Peterca, M. R. Imam, V. Percec, *Chem. Rev.* **2009**, *109*, 6275–6540.

**6** J. Roosma, T. Mes, P. Leclere, A. Palmans, E. W. Meijer, *J. Am. Chem. Soc.* **2008**, *130*, 1120–1121.

**7** V. Percec, A. E. Dulcey, M. Peterca, M. Ilies, M. J. Sienkowska, P. A. Heiney, *J. Am. Chem. Soc.* **2005**, *127*, 17902–17909.

**8** K. L. Zhong, T. Chen, B. Yin, L. Y. Jin, *Macromol Res.* **2009**, *17*, 280–283.

**9** C. Wang, Y. Guo, Z. Wang, X. Zhang, *Langmuir* **2010**, *26*, 14509–14511.

**10** M. Smulders, A. P. Schenning, E. W. Meijer, *J. Am. Chem. Soc.* **2008**, *130*, 606–611.

**11** S. D. Starnes, S. Arungundram, C. H. Saunders, *Tetrahedron Lett.* **2002**, *43*, 7785–7788.

**12** H.-J. Kim, Y.-H. Jeong, E. Lee, M. Lee, *J. Am. Chem. Soc.* **2009**, *131*, 17371–17375.

**13** V. Percec, J. G. Rudick, M. Peterca, P. A. Heiney, *J. Am. Chem. Soc.* **2008**, *130*, 7503–7508.

**14** J. Motoyanagi, T. Fukushima, N. Ishii, T. Aida, *J. Am. Chem. Soc.* **2006**, *128*, 4220–4221.

**15** M. Lee, B.-K. Cho, N.-K. Oh, W.-C. Zin, *Macromolecules* **2001**, *34*, 1987–1995.

**16** I. W. Hamley, V. Castelletto, Z. B. Lu, C. T. Imrie, T. Itoh, M. Al-Hussein, *Macromolecules* **2004**, *37*, 4798–4807.

**17** E. Lee, J. K. Kim, M. Lee, *Angew. Chem., Int. Ed.* **2008**, *47*, 6375–6378.

**18** V. Percec, M. Lee, *J. Mater. Chem.* **1992**, *2*, 617–623.

**19** J. G. Rudick, V. Percec, *New J. Chem.* **2007**, *31*, 1083–1085.

**20** L. B. Liu, K. S. Moon, R. Gunawidjaja, E. Lee, V. Tsukruk, M. Lee, *Langmuir* **2008**, *24*, 3930–3936.

**21** C. Lavigueur, E. J. Foster, V. E. Williams, *Liq. Cryst.* **2007**, *34*, 833–840.

**22** E. Voisin, J. E. Foster, M. Rakotomalala, V. E. Williams, *Chem. Mater.* **2009**, *21*, 3251–3261.

**23** D.-J. Hong, H. Jeong, J.-K. Lee, W.-C. Zin, T. D. Nguyen, S. C. Glotzer, M. Lee, *Angew. Chem., Int. Ed.* **2009**, *48*, 1664–1668.

**24** J. Wu, W. Pisula, K. Müllen, *Chem. Rev.* **2007**, *107*, 718–747.

**25** K. L. Zhong, Z. Huang, Z. Man, L. Y. Jin, B. Yin, M. Lee, *J. Polym. Sci., Part A: Polym. Chem.* **2010**, *48*, 1415–1422.

**26** Y. Shirai, A. J. Osgood, Y. Zhao, Y. Yao, L. Saudan, H. Yang, Y.-H. Chiu, L. Alemany, B. T. Sasaki, J.-F. Morin, J. M. Guerrero, K. F. Kelly, J. M. Tour, *J. Am. Chem. Soc.* **2006**, *128*, 4854–4864.

**27** L. C. Palmer, S. I. Stupp, *Acc. Chem. Res.* **2008**, *41*, 1674–1684.

**28** W. C. Zin, B. K. Cho, M. Lee, *Chem. Rev.* **2001**, *101*, 3869–3892.

**29** E. Lee, Z. Huang, J.-H. Ryu, M. Lee, *Chem. Eur. J.* **2008**, *14*, 6957–6966.

**30** S. Li, Z. He, J. Yu, S. Chen, A. Zhong, R. Tang, H. Wu, J. Qin, Z. Li, *J. Mater. Chem.* **2012**, *22*, 12523–12531.

**31** K. Zhong, Z. Man, Z. Huang, T. Chen, B. Yin, L. Y. Jin, *Polym. Int.* **2011**, *60*, 845–850.

**32** L. R. Tian, K.-L. Zhong, Y. J. Liu, Z. G. Huang, L. Y. Jin, L. S. Hirst, *Soft Matter* **2010**, *6*, 5993–5998